Accepted for publication in Ocean Engineering 21/05/2019
https://doi.org/10.1016/j.oceaneng.2019.05.044

Applicability of the strain accumulation procedure for the geotechnical foundation design of zero-radius bend triggers

Author 1

- Dimitra Zografou, PhD
- Aurecon. Formerly Centre for Offshore Foundation Systems, The University of Western Australia.

Author 2

- Susan Gourvenec, Professor
- School of Engineering, University of Southampton, UK. Formerly of Centre for Offshore Foundation Systems, The University of Western Australia

Author 3

- Conleth O'Loughlin, Associate Professor
- Centre for Offshore Foundation Systems, The University of Western Australia

Author 4

- Meysam Banimahd, PhD
- The University of Western Australia

Full contact details of corresponding author

- Email: dimitra.zografou@gmail.com

- Address: Centre for Offshore Foundation Systems
  The University of Western Australia (M053)
  35 Stirling Highway
  CRAWLEY WA 6009
  Australia

Abstract

Accepted for publication in Ocean Engineering 21/05/2019
https://doi.org/10.1016/j.oceaneng.2019.05.044

Geotechnical design of offshore shallow foundations is generally based on a cyclically degraded shear strength, typically determined from a shear strain or pore pressure accumulation procedure based on contour diagrams derived from laboratory tests. The procedure was initially developed for gravity-based structures and is now used for a wider range of offshore applications including shallow foundations for subsea structures that are subjected to different cyclic loading regimes. The applicability of the traditional equivalent cyclic shear strength approach based on the accumulation procedure is investigated for a specific type of subsea structure, the Zero-Radius Bend (ZRB) trigger. A series of centrifuge tests have been performed on a shallow skirted foundation on normally consolidated kaolin clay under a range of horizontal cyclic load sequences typical of those applied to foundations of ZRB triggers during pipe-laying. The observed performance from the centrifuge tests is compared with predictions of foundation performance using the traditional strain accumulation procedure. It is shown that the traditional procedure over predicts strength degradation at the end of the particular cyclic load sequences. The findings indicate that a performance-based approach may be more appropriate for the geotechnical design of these foundations and other foundations with a high tolerance to displacement.

KEYWORDS: shallow foundations; cyclic loading; centrifuge modelling.

List of notation

A	foundation base area
A_s	skirt wall surface area
A_{sp}	area of soil plug
A_{tip}	plan area of the skirt tips
c_h	horizontal coefficient of consolidation
c_v	vertical coefficient of consolidation
D	diameter
d	skirt depth
d/D	embedment ratio
$D_{T\text{-}bar}$	T-bar diameter
F_{bs}	soil buoyancy

Accepted for publication in Ocean Engineering 21/05/2019
https://doi.org/10.1016/j.oceaneng.2019.05.044

F_{bw}	water buoyancy
g	standard gravity
G_s	specific gravity
h	horizontal displacement
k	undrained shear strength gradient
LL	liquid limit
M	critical state friction constant
N	number of cycles
N_{c0}	bearing capacity factor
N_{eq}	equivalent number of cycles
N_g	centrifuge acceleration
N_p	lateral bearing capacity factor
$N_{T\text{-}bar}$	T-bar capacity factor
PL	plastic limit
q_H	horizontal stress
$q_{H,ave}$	average horizontal stress
$q_{H,cyc}$	cyclic horizontal stress
$q_{H,max}$	maximum horizontal stress
$q_{H,ult}$	ultimate horizontal capacity of foundation
q_m	measured resistance
q_{net}	net geotechnical resistance
$q_{net,i}$	net geotechnical installation resistance
$q_{net,i,theor}$	theoretical prediction of net geotechnical installation resistance
$q_{net,theor}$	theoretical net geotechnical resistance
q_V	vertical stress
$q_{V,ult}$	ultimate vertical capacity of foundation
s_u	undrained shear strength/ monotonic DSS strength
$s_{u,ave}$	average undrained shear strength over embedment depth
s_{u0}	undrained shear strength at the skirt tip
s_{um}	undrained shear strength at mudline
t	skirt thickness

Accepted for publication in Ocean Engineering 21/05/2019
https://doi.org/10.1016/j.oceaneng.2019.05.044

v	velocity
w	vertical displacement
W'_{sp}	submerged weight of soil plug
$W_{\Delta g}$	increase of self weight of foundation
z	depth
α	interface friction factor
γ'	effective unit weight
γ_{max}	maximum shear strain
κ	recompression index
λ	virgin compression index
ν	Poisson's ratio
σ'_{v0}	effective vertical stress at skirt tip level
τ_{ave}	average shear stress
τ_{cyc}	cyclic shear stress
τ_{max}	maximum shear stress

Accepted for publication in Ocean Engineering 21/05/2019
https://doi.org/10.1016/j.oceaneng.2019.05.044

1 Introduction

Shallow foundations for offshore applications are typically sized by considering an ultimate limit state based on a cyclically degraded undrained shear strength, $s_{u,cyc}$. The cyclic shear strength is determined for an appropriate - 'equivalent' - number of cycles, N_{eq}, determined from an accumulation procedure based on shear strain (or excess pore pressure ratio) contours derived from laboratory element test data (Andersen 2015). The method was originally developed for gravity-based fixed platforms under environmental loading, but is increasingly applied to design of shallow foundation systems for subsea structures that are subjected to different cyclic loading regimes, often dominated by installation and operational loads. Shallow foundations for some types of subsea structures may also have a higher tolerance to displacement than a foundation for a fixed platform enabling redefinition of the traditional basis of design. This paper presents the results of an investigation into the applicability of the traditional strain accumulation procedure for the assessment of the effect of cyclic loading on a particular type of subsea structure, a Zero-Radius Bend (ZRB) trigger.

ZRB triggers are one approach to manage controlled buckling of subsea pipelines (Bruton et al. 2006, 2008). The ZRB method is increasingly adopted globally as it has advantages over the snake-lay method of buckle control that may result in undesirable pipe embedment and over vertical upsets as it does not lead to asymmetric buckles and induces lower compressive forces (Peek & Kristiansen 2009).

A ZRB trigger comprises a shallow foundation with vertical post, as seen in Figure 1, and facilitates the pipeline being laid with an infinitesimal pipeline curvature. The ZRB pipe laying procedure comprises three key stages, which are shown schematically on

Figure 2 and Figure 3 and described below.

Stage 1: The pipe-laying vessel lays the pipeline across the ZRB trigger at a distance from the vertical post.

Stage 2: The vessel moves laterally so that a small pipeline curvature is created and the pipeline is eventually pulled towards the vertical post of the ZRB trigger.

Stage 3: The vessel moves forward and the pipe-laying procedure continues.

Accepted for publication in Ocean Engineering 21/05/2019
https://doi.org/10.1016/j.oceaneng.2019.05.044

A ZRB trigger foundation is subjected to horizontal cyclic loading during pipe-laying caused by intermittent contact between the pipeline and the vertical post. Figure 4 shows typical horizontal stress, q_H, with the number of cycles, N, during the three pipe-laying stages, together with the average horizontal stress, $q_{H,ave}$, cyclic horizontal stress $q_{H,cyc}$ and maximum horizontal stress $q_{H,max}$ within a cycle. Figure 4 shows that $q_{H,ave}$ is lowest during Stage 1 and increases linearly with cycles during Stage 2 to a maximum value that is maintained during Stage 3. The cyclic component of horizontal stress is approximately constant during the three stages, with the exception of the start of Stage 2, when the horizontal stresses reach their maximum values over a short time interval as the pipeline is pulled abruptly towards the vertical post. The frequency of the cyclic loading is generally dictated by dominant wave periods between 8 s and 14 s and is expected to result in an undrained soil response for typically dimensioned ZRB triggers in soft seabed sediments. ZRB foundations have a high tolerance to horizontal displacement, h, able to displace in the order of several metres and still perform their intended function.

The scope of the present study was to investigate the applicability of the traditional cyclically degraded strength approach, based on the shear strain accumulation procedure, for the geotechnical design of ZRB foundations. Results of a series of centrifuge tests on a shallow skirted foundation in normally consolidated kaolin clay involving cyclic loading typical of ZRB foundations during pipe-laying are presented. Observations are compared with predictions of foundation performance using the accumulation procedure and strain contour diagrams developed from a suite of cyclic direct simple shear tests on kaolin clay.

2 Centrifuge Experiments

2.1 Experimental arrangement

The experiments were performed in a 1.8 m radius fixed beam centrifuge at National Geotechnical Centrifuge Centre at the University of Western Australia (Randolph et al. 1991).

Accepted for publication in Ocean Engineering 21/05/2019
https://doi.org/10.1016/j.oceaneng.2019.05.044

The model foundation was connected to the vertical axis of a two-dimensional electrical actuator (see Figure 5), with the cyclic loading achieved using the horizontal axis of the actuator under load control. The foundation was fabricated as circular in cross section with a diameter, D = 60 mm, a skirt depth, d = 12 mm, and therefore an embedment ratio, d/D = 0.2 and with a skirt thickness, t = 0.48 mm such that the equivalent prototype foundation at 200g has D = 12 m, d = 2.4 m and t = 0.096 m. The prototype foundation dimensions were chosen as representative of those of ZRB foundations. The foundation was equipped with a vent in the top cap to allow drainage of the water from inside the skirt during installation. As the foundation was fabricated from aluminium rather than steel, a realistic foundation self-weight was replicated by controlling the vertical load on the foundation using the vertical axis of the actuator.

2.2 Sample preparation and strength profile

The tests were carried out in a well-characterised normally consolidated kaolin clay with properties as shown in Table 1 (Stewart 1992). Soft normally consolidated kaolin clay is considered to have a soil strength that is representative of soft seabed sediments and has been used extensively in modelling of offshore geotechnical problems over the last three decades (e.g. Dunnavant and Kwan 1993, Dean et al. 1998, Dingle et al. 2008, Zakeri et al. 2014, Yuan et al. 2017). The sample was prepared from a kaolin slurry prepared at twice the liquid limit in a strong box with internal dimensions 390 × 650 × 325 mm (width × length × depth). A 20 mm layer of sand was placed at the bottom of the sample container before pouring the slurry to allow two-way drainage during consolidation. Geotextile drains were also located at each corner of the sample to provide a hydraulic connection between the bottom drainage layer and the free water at the sample surface. The sample was consolidated in the centrifuge at 200 g for 3.5 days. A 40 mm water layer was maintained at the sample surface during consolidation and over the course of testing to ensure sample saturation. After consolidation, a thin layer was scraped from the sample surface, ranging from 0 mm at the middle to 10 mm at the edges, to ensure a level testing surface and to create a final sample height of approximately 170 mm. The sample was then re-spun for a period of 3 hours before the sample characterisation tests commenced.

Accepted for publication in Ocean Engineering 21/05/2019
https://doi.org/10.1016/j.oceaneng.2019.05.044

Table 1 Typical properties of kaolin clay

Property	Value	
Liquid limit, LL (%)	61	Stewart 1992
Plastic limit, PL (%)	27	
Specific gravity, G_s	2.6	
Poisson's ratio, v	0.30	
Critical state friction constant, M	0.92	
Virgin compression index, λ	0.205	
Recompression index, κ	0.044	
c_v (σ'_{vo} = 13 kPa)	1.5 m^2/ year	Cocjin et al. 2014,
c_h (σ'_{vo} = 13 kPa)	6.6 m^2/ year	Colreavy et al. 2016

The sample was characterised through T-bar penetrometer tests (Stewart & Randolph 1991) using a model T-bar with a diameter, $D_{T\text{-}bar}$ = 5 mm. The T-bar was inserted and extracted at a velocity, v = 1 mm/s, satisfying the undrained criterion, $D_{T\text{-}bar}v/c_v > 30$ (Finnie & Randolph 1994). The undrained shear strength, s_u, was calculated from the measured penetration resistance using the commonly adopted T-bar bearing factor, $N_{T\text{-}bar}$ = 10.5 (e.g. Colreavy et al. 2016). A cyclic T-bar test was performed at a depth of 50 mm, by vertically cycling the T-bar through ± 10 mm ($2D_{T\text{-}bar}$). This provided a basis for correcting the measured T-bar resistance for soil buoyancy, the changing self-weight (with radius) of the load cell and T-bar probe (as described in Sahdi et al. 2014), and for estimating the fully remoulded undrained shear strength.

Profiles of s_u with prototype depth, z, derived from the T-bar tests are provided in Figure 6, both before and after the foundation tests. Over the entire penetration depth, s_u can be idealised as $s_u = s_{um} + kz$, where the undrained shear strength at the mudline, s_{um} = 0 kPa, and the gradient of undrained shear strength with depth, k = 0.75 kPa/m before testing and k = 0.91 kPa/m after testing. Figure 6 also includes s_u profiles from T-bar tests conducted in a foundation footprint to quantify strength changes due to consolidation from the vertical load maintained on the foundation during the cyclic tests, as discussed later.

2.3 Experimental programme and load application

The experimental programme included two monotonic tests and five cyclic tests under one-way horizontal cyclic loading. Monotonic tests were performed to define the ultimate vertical capacity, $q_{V,ult}$, and the ultimate horizontal capacity, $q_{H,ult}$, of the foundation. The vertical stress, q_V, and horizontal

stress, q_H, equal to the applied vertical load and horizontal load respectively divided by the foundation base area, were applied in the cyclic tests as a percentage of the monotonic $q_{V,ult}$ and $q_{H,ult}$ respectively. Details of the tests are provided in Table 2 and a schematic representation of the cyclic horizontal stress sequences is presented in Figure 7. The sign convention used in the model tests for stress and displacement, including vertical displacement, w, is illustrated in Figure 2.

The monotonic tests were performed under displacement control and the cyclic tests were performed under load control. Horizontal and vertical loading was applied to the model foundation via a rigid loading arm, strain-gauged, such that the horizontal loading could be derived from the measured bending moments.

Table 2 Summary of centrifuge test sequences

Brief description	**Test label**	**Normalised horizontal stress ($q_{H,ave}$ +/- q_{Hcyc}) /$q_{H,ult}$**	**No. of cycles N**
Monotonic vertical	V	-	-
Monotonic horizontal	H	-	-
Representing conditions applied on ZRB foundation: Non-uniform horizontal cyclic load sequence with 3 stages of cyclic loading during pipe-laying with 3 high instant loads applied at beginning of stage 2	ZRBp	0.15 ± 0.15 (S1u equivalent) 0.60 ± 0.40 (Peaks) 0.40 ± 0.25 (Peaks) 0.15 to 0.60 ± 0.15 (S2u equivalent) 0.60 ± 0.15 (S3u equivalent)	360 1 2 357 1080
Representing conditions applied on ZRB foundation: Non-uniform horizontal cyclic load sequence with 3 stages of cyclic loading during pipe-laying with 3 high instant loads applied at beginning of stage 2	ZRB	0.15 ± 0.15 (S1u equivalent) 0.15 to 0. 60 ± 0.15 (S2u equivalent) 0.60 ± 0.15 (S3u equivalent)	360 360 1080
Uniform horizontal cyclic load sequence of same magnitude as Stage 1 in ZRB sequence	S1u	0.15 ± 0.15	1800
Uniform horizontal cyclic load sequence of same magnitude as average of Stage 2 in test ZRB	S2u	0.35 ± 0.15	1800
Uniform horizontal cyclic load sequence of same magnitude as Stage 3 in ZRB sequence	S3u	0.60 ± 0.15	1800

The monotonic vertical test involved vertical extraction of the foundation until the skirt was free of the mudline, while the horizontal test involved lateral displacement of the foundation for a distance of approximately 0.1 D, sufficient to mobilise a steady state. These tests were performed at a velocity,

v = 0.1 mm/s ensuring that the dimensionless ratios, $D.v/c_v$ and $D.v/c_h$, were both greater than 30 and undrained conditions were achieved (Finnie & Randolph 1994) (c_v and c_h are the vertical and horizontal coefficients of consolidation respectively as quantified in Table 1).

Cyclic horizontal loading was applied under a constant vertical load, using sinusoidal cycles of horizontal load with an amplitude as detailed in Table 2 and at a frequency of 0.25 Hz. This frequency was selected to ensure the response was undrained, whilst maintaining high quality load control (noting that this is limited by the mechanical speed of the actuator and the update frequency of the feedback loop, and also governed by the proportional–integral–derivative controller settings). The dissipation of excess pore pressure in a given cycle was less than 20%, which is sufficiently low to achieve undrained conditions (Osman & Randolph 2012).

Each of the five cyclic tests involved 1800 cycles, which is representative of the typical loading experienced by a ZRB foundation during pipe-laying. Three of the cyclic tests involved uniform cyclic loading, with average and cyclic load amplitudes that simulate those in each stage of a ZRB loading sequences, albeit that the ramp in the average cyclic load in Stage 2 was simplified as an average cyclic load for the uniform amplitude test. The remaining two cyclic tests involved load sequences that were idealised forms of the non-uniform sequences experienced by the foundation of a ZRB trigger during pipe-laying, with and without the three cycles of high lateral load at the beginning of Stage 2 (see Figure 4). Collectively the five cyclic tests allow the effects of stress history to be examined.

2.4 Foundation Installation Procedure

The foundation was installed with the drainage vent open at a velocity of 0.1 mm/s to target undrained conditions ($Dv/c_v > 30$). Installation was continued until the underside of the foundation top plate made contact with the mudline, as indicated by a sharp increase in the vertical load. The actuator was then set to maintain the foundation at the final installation depth, and the centrifuge was stopped for approximately 5 minutes to seal the vent. After restarting the centrifuge and spinning at the 200 g target acceleration, the actuator was switched to load control to target a vertical load of 13 N (q_v = 4.6 kPa), except for the monotonic pullout test (V) where a vertical load of 9 N (q_v = 3.2 kPa) was applied. The

vertical load was held for a period of approximately 13 minutes (1 year in prototype scale) before commencing the horizontal cyclic loading part of the test.

3 Centrifuge Test Results

3.1 Foundation Installation Resistance

The measured resistance, q_m, equal to the measured load divided by the foundation base area, during foundation installation is presented in Figure 8 (a). As expected from the linear profile of s_u with depth, q_m, increases approximately with depth until z/d ≈1 when the foundation top plate makes contact with the mudline. The net geotechnical installation resistance, $q_{net,i}$, can be determined as:

$$q_{net,i} = q_m - \left(\frac{F_{bs} + F_{bw} - W_{\Delta g}}{A}\right) \qquad (1)$$

where F_{bs} is the soil buoyancy due to the soil displaced by the penetrating skirts (equal to the product of the embedded skirt volume and the effective unit weight, γ', which over the skirt length averages γ' = 5.9 kN/m^3 as established from post-test measurements of moisture content), F_{bw} is the water buoyancy due to the increasing length of the rod submerged in the free water above the soil sample (equal to the product of the volume of the submerged rod and the unit weight of water), $W_{\Delta g}$ is the increase in foundation self weight due to the slight variation in centrifuge acceleration with embedment, and A is the foundation base area.

Profiles of measured and net geotechnical resistance during foundation installation for a typical test [ZRBp] are presented on Figure 8 (b) together with the theoretical prediction of geotechnical resistance

$$q_{net,i,theor} = [A_s.\alpha.s_{u,ave} + A_{tip}.(N_{C0}.s_{u0} + \gamma' N_g z)]/A \qquad (2)$$

where A_s is the skirt wall surface area (internal and external), α is the interface friction ratio (taken as α = 0.4, as quantified from the ratio of the final remoulded penetration resistance to the intact penetration resistance in the cyclic T-bar test), $s_{u,ave}$ is the average value of undrained shear strength over the current embedment depth, s_{u0} is the undrained shear strength at the skirt tip, A_{tip} is the plan area of the skirt tips,

N_{c0} is a bearing capacity factor taken as N_{c0} = 7.5 for a buried strip foundation in uniform clay (Skempton 1951) and N_g is the centrifuge acceleration at the current skirt tip level.

Figure 8 (b) shows that the net resistance is slightly lower than the theoretically predicted resistance, which can suggest that the soil strength mobilised along the skirts is lower than the remoulded strength value predicted by the cyclic T-bar test. This is consistent with water entrainment at the skirt-soil interface, as observed in other experimental studies (e.g. Tika & Hutchinson 1999, Gaudin et al. 2014, O'Beirne et al. 2017, Yuan et al. 2017). A best fit is achieved if a value of α = 0.2 is assumed.

3.2 Undrained vertical resistance

The resistance in undrained uplift and compression is expected to be similar if reverse end bearing is mobilised (Mana et al. 2012, Mana et al. 2013a) and a pullout test was selected to minimise disturbance to the sample. Figure 9 shows the measured uplift resistance of the foundation, q_m, along with the net geotechnical resistance, q_{net} (Equation 3), i.e. adjusted to account for soil and water buoyancy, the changing weight of the foundation with depth, and the difference between the overburden pressure and the submerged weight of the soil plug (Tani & Craig 1995).

$$q_{net} = q_m - \left(\frac{F_{bs} + F_{bw} - W_{\Delta g} - W'_{sp} + A_{sp}\,\sigma'_{v0}}{A}\right) \qquad (3)$$

where σ'_{v0} is the effective vertical stress at the skirt tip level (equal to $\gamma' N_g z$), W'_{sp} is the submerged weight of the soil plug that is confined by the skirts, A_{sp} is the area of the soil plug, and the remaining components are as defined previously.

Also shown on Figure 9 is the theoretically predicted resistance,

$$q_{net,theor} = N_{c0}.s_{u0} \qquad (4)$$

where the capacity factor was taken as N_{c0} = 10.9 as appropriate for kD/s_{um} = 200 and an embedment ratio, d/D = 0.2 (Gourvenec & Mana 2011). Predictions of the vertical capacity are shown based on both initial and final undrained shear strengths, derived from T-bar tests conducted before and after the foundation uplift tests, see Figure 6). Good agreement with the measured uplift resistance is obtained

when using the final undrained shear strength at the skirt tip, s_{u0} = 2.1 kPa ; The measured ultimate undrained vertical resistance, $q_{V,ult}$, of the foundation is equal to 24 kPa while the theoretically predicted resistance based on the final undrained shear strength, $q_{net,theor}$ (final s_u), is equal to 23 kPa. The increase of s_{u0} is discussed in more detail later in the paper. The ultimate undrained vertical resistance of the foundation is taken as $q_{V,ult}$ = 24 kPa and the targeted vertical (compressive) load applied to the foundation in the horizontal monotonic and cyclic tests was $0.2q_{V,ult}$.

3.3 Ultimate horizontal resistance

Figure 10 shows the mobilisation of horizontal resistance through horizontal translation under a constant vertical stress of 0.2 $q_{V,ult}$. The horizontal resistance reached a maximum, and steady state, at $q_{H,ult}$ = 4.2 kPa at a normalised horizontal displacement, h/D ~ 2%. Real time video footage confirmed that a gap did not form at the trailing edge of the foundation during the test, as expected for the given undrained shear strength ratio of the material (Britto & Kusakabe, 1982, Mana et al., 2013b).

Also shown on Figure 10 is the theoretical ultimate horizontal resistance given by equation (5).

$$q_{H,ult,theor} = s_{u0} + \frac{d.D.N_p.s_{u,ave}.}{A} \qquad (5)$$

where the first term represents the contribution of base shear and the second term represents the active and passive resistance, in which the lateral bearing capacity factor is taken as N_p = 5.66 for a two-sided mechanism consistent with no gap developing (Caquot & Kerisel, 1948). As with the uplift tests, predictions of horizontal capacity are based on both the initial and final undrained shear strengths, with the best agreement obtained using the final undrained shear strength consistent with the uplift tests. The observed ultimate horizontal resistance, $q_{H,ult}$ = 4.2 kPa, provided the basis for selecting the average and cyclic horizontal stress in the cyclic tests.

3.4 Response of foundation under cyclic load sequences

Figure 11 presents the measured normalised horizontal displacements due to uniform cyclic stress sequences of magnitude similar to each of the stages of the ZRB sequence [S1u, S2u and S3u] and the ZRB cyclic stress sequence without the instantaneous peak loads at the transition of Stages 1 and 2 [ZRB]. Displacements are shown at the start of Stage 1 ((a) N = 0-50); across the transition between

Stage 1 and 2 ((b) N = 355-405); across the transition between Stage 2 and 3 ((c) N = 715-765); and within Stage 3 towards the end of the test ((d) N = 1700-1750). The applied normalised horizontal stresses, $q_H/q_{H,ult}$, are as presented in Figure 7.

The horizontal displacements at each stage in the ZRB test are similar to those observed in the uniform test of equivalent magnitude. This observation also applies when comparing the test with uniform amplitude equivalent to the mean of Stage 2 [S2u] with the increasing $q_{H,ave}$ in Stage 2 of the ZRB sequence where the horizontal displacements appear indistinguishable at the transition from Stage 2 to 3. However, an exception is the comparison between the test with a uniform load equivalent to Stage 1 [S1u], in which the displacements are higher than the equivalent displacements in the ZRB test, due to an applied $q_{H,ave}$ that was unintentionally higher than the target value. As a result, the final horizontal displacement at the end of the ZRB test is similar to that at the end of the test with uniform horizontal stress equal to the Stage 3 amplitude. The magnitude of the final horizontal displacement appears therefore to be governed by the magnitude of $q_{H,ave}$ and not by stress history.

Figure 12 examines the effect of the high instantaneous stresses at the beginning of Stage 2 in test ZRBp by comparing the horizontal displacements observed in the ZRB sequence without the high instantaneous stresses with those in the test with a uniform sequence equivalent to Stage 3 [S3u]. The response of the foundation is stable in the three tests and does not show any signs of failure. The final horizontal displacements are similar for the three tests despite differences in the stress history. Application of the instantaneous high stresses resulted in a corresponding instantaneous increase in h_{max}/d of 3.7% and a permanent increase of 0.9%, although the final horizontal displacement at the end of the final load sequence was unaffected. This may be attributed to h_{max} induced by the high instantaneous stresses being lower than h_{max} induced by $q_{H,ave}$ in the final stage of the ZRB sequence. It appears therefore, that the final horizontal displacement is dictated by the maximum $q_{H,ave}$ applied in Stage 3, irrespective of the presence of the high instantaneous stresses at the transition between Stages 1 and 2.

Accepted for publication in Ocean Engineering 21/05/2019
https://doi.org/10.1016/j.oceaneng.2019.05.044

3.5 Assessment of centrifuge background consolidation

Background consolidation of the clay sample takes place during centrifuge testing more rapidly than in the field as the drainage path lengths in the centrifuge sample are N_g^2 lower than in the field. This is the basis for the N_g^2 scaling applied to consolidation times when scaling from the centrifuge to prototype conditions (Garnier et al. 2007). This is generally beneficial in centrifuge modelling as modelling processes involving dissipation of excess pore water pressures are relatively fast. However, in the modelling considered here, the (relatively) quicker consolidation leads to soil strength gains that are more rapid than would occur in the field. The overall time period for the lay process in the centrifuge was two hours, corresponding to approximately nine years at prototype scale, compared with a typical pipe laying over a ZRB duration in the field of a few hours. To assess if the effect of background consolidation that occurred over this prolonged testing duration had a significant effect on the increase of undrained shear strength s_u of the sample during a cyclic foundation test, and therefore on the magnitude of the normalised applied loads, T-bar tests were performed before and after the foundation tests. As shown by Figure 6, the final T-bar tests were conducted both at untested sites and through the foundation footprints to permit temporal changes in sample strength to be distinguished from strength changes due to consolidation from the vertical load applied to the foundation. Figure 6 shows that the undrained shear strength at skirt tip level s_{u0} increases from 1.7 kPa to 2.1 kPa over the course of the test campaign (comparing s_u profiles before and after testing), but that the horizontal cyclic shear stresses caused negligible additional increases above or around the skirt tip level (comparing s_u profiles in tested and undisturbed sites). However, there is an additional increase in s_u in the test footprint below skirt tip level, which is attributed to consolidation from the vertical load applied to the foundation over each two hour cyclic test. The magnitude of the measured s_u increase is approximately 20%, which is consistent with the prediction from a theoretical critical state framework for consolidated gains of shallow foundation capacity proposed by Gourvenec et al. (2014) and extended to embedded circular foundations by Vulpe et al. (2017).

The s_u increase is expected to have taken place towards the beginning of the test campaign as evidenced by the monotonic test (conducted early in the test programme) in which the horizontal resistance was

in good agreement with the theoretical resistance based on the final undrained strength. As $q_{H,ult}$ is not considered to increase significantly after the monotonic test and given that there is negligible increase in s_u after testing through the foundation footprint as discussed above, the effect of background consolidation in the cyclic tests is not considered to be significant and the applied ratios $q_H/q_{H,ult}$ can be considered equal to the target values during the cyclic tests.

4 Prediction of foundation response from accumulation procedure

The observed response of the foundation in the centrifuge tests is compared with predictions based on the strain accumulation procedure. The strain contour diagrams were derived from stress-controlled cyclic direct simple shear (DSS) tests under two-way symmetrical (with $\tau_{ave}= 0$, where τ_{ave} is the average shear stress) and one-way non-symmetrical cyclic loading (with $\tau_{ave} = \tau_{cyc}$, where τ_{cyc} is the cyclic shear stress) on normally consolidated kaolin (i.e. the same material as used in the centrifuge tests) as described fully in Zografou et al. (2019). Although soil elements below a shallow skirted foundation under horizontal translation are expected to experience various stress conditions, DSS tests were chosen as the representative of the average response.

For the accumulation procedure, the ZRB sequences must be transformed into parcels of uniform cyclic stress in ascending order. This can be approximated as either (a) symmetrical cyclic loading of parcels with τ_{max} equal to 0.5 $q_{H,max}/q_{H,ult}$ of the ZRB sequences, where τ_{max} is the maximum shear stress, or (b) non-symmetrical cyclic loading with parcels of τ_{max}/s_u equal to $q_{H,max}/q_{H,ult}$ of the ZRB sequences. The idealised cyclic load sequences to represent tests ZRB and ZRBp are illustrated schematically in Figure 13. It is noted that to account for the increasing q_H/q_{Hult} in Stage 2, the average value of q_H/q_{Hult} is considered in the second parcel. Neither idealisation is ideal since in the symmetrical case the average stress ratios cannot be captured, maximum stress ratios are lower and the cyclic stress ratios are higher than in the actual ZRB sequences; while in the non-symmetrical case the maximum stress ratios are captured but the average stress ratios are lower and the cyclic stress ratios are higher than in the actual ZRB sequences in Stages 2 and 3.

The strain accumulation for the idealised sequences for tests ZRB and ZRBp are presented on contour diagrams of maximum shear strain, γ_{max}, for both symmetrical and non-symmetrical cyclic loading in Figure 14 and Figure 15 respectively. The accumulation procedure for the ZRB sequence with and without the high instantaneous peak loads intersects the failure envelope during the penultimate or final package with the final stress state lying beyond the failure envelope. The non-symmetrical cyclic load idealisation leads to the final position of both the ZRB and ZRBp tests falling further beyond the failure envelope compared to the symmetrical loading idealisation. Cyclic strength reduction factors, $s_{u,cyc}/s_{u,}$ of approximately 0.6 and 0.25 are inferred from Figure 14 and Figure 15 for the symmetrical and non-symmetrical cyclic stress sequence idealisations respectively, and notably achieved before completion of the cyclic stress sequences. The failure envelopes for the two cyclic stress conditions considered are defined by the 5% and 25% shear strain contours under symmetrical and non-symmetrical cyclic loading respectively, based on observations from the cyclic DSS tests, discussed in detail in Zografou et al. (2019).

The implications from the strain accumulation procedure are contrary to those from the centrifuge tests in which all the tests showed a stable response, i.e. no further displacement with increasing number of cycles at constant stress level, and with final horizontal displacements less than 2% of the foundation diameter at the end of the pipe laying installation sequence.

Results from this analysis indicate that cyclically reduced shear strength at a prescribed value of shear strain based on data from soil element tests, may not be a representative criterion to define the 'failure' of a ZRB foundation. The critical design criterion for ZRB foundations may be better defined in terms of horizontal displacement and not soil strength reduction.

5 Comparison with response of equivalent DSS tests

In this section the observed displacements of the foundation centrifuge model are compared with shear strains developed during cyclic DSS tests with normalised shear stresses, τ/s_u, similar to the normalised horizontal stresses, $q_H/q_{H,ult}$, applied in the centrifuge tests. The shear-strain response in the cyclic DSS tests is illustrated in Figure 16.

From Figure 11 and Figure 16, a comparison can be made between the response in the centrifuge tests with uniform horizontal cyclic stress sequences representing the three stages of the ZRB loading sequence (S1u, S2u and S3u) and in the equivalent cyclic DSS tests (Cns1, Cns7 and Cns8). The form of the normalised displacement response in the foundation centrifuge test is similar with the strain response in the DSS tests, in that the horizontal displacements and strains stabilise after the application of the average horizontal or shear stress or after a few hundreds of cycles of loading. Several studies based on cyclic simple shear and triaxial tests have shown a threshold of cyclic shear stress below which failure does not occur even at a high number of cycles (e.g. Vucetic 1994, Larew & Leonards 1962). Similarly, it has been shown for offshore piles, based on field tests in a range of clays and sands, that there is an envelope or combinations of average and cyclic axial loads, identified as a stable zone, for which axial displacements stabilise or develop very slowly for over 1000 cycles (Jardine et al. 2012, Jardine & Standing 2012, Tsuha et al. 2012, Rimoy et al. 2013). The stable zone, referred to as the threshold stress or 'shakedown', has also been identified by numerical and analytical solutions (Levy et al. 2009, Krabbenhoft et al. 2007). The findings of the present study indicate that there is a threshold stress for shallow skirted foundations under horizontal cyclic loading and that DSS tests may be appropriate to identify the threshold by equating τ/s_u in the element test with $q_H/q_{H,ult}$ in the foundation test.

6 Concluding remarks

A suite of centrifuge tests was performed on a shallow skirted foundation in normally consolidated kaolin clay under a range of horizontal cyclic stress sequences typical of foundations of ZRB triggers during pipe-laying. The observed performance from the centrifuge tests was compared with theoretical predictions using the traditional strain accumulation procedure on contour diagrams from cyclic DSS tests. The strain accumulation procedure indicated that the modelled foundation load sequence would lead to failure but this was not evidenced from the observed foundation response in the centrifuge tests suggesting that the shear strain accumulation procedure may not be suitable to assess the foundation response of ZRB triggers. This is partly attributed to the difficulty in idealising the ZRB sequences into

parcels of uniform amplitude in ascending order to suit the strain accumulation procedure; and partly due to the failure criterion based on soil element tests not being representative for the failure of a structure such as a ZRB trigger that has a high tolerance to horizontal displacement.

The foundation response in the centrifuge and the soil response in cyclic DSS tests performed at τ/s_u similar to the ratios of $q_H/q_{H,ult}$ in the stages of ZRB sequences showed a stable response. The foundation response in the centrifuge appeared to depend on the last stage of ZRB sequence, with the highest ratio of $q_H/q_{H,ult}$, rather than the previous stages or stress history. Cyclic DSS tests appear potentially suitable to define a threshold stress, or combination of average and cyclic stress, below which the foundation maintains a stable response.

Results from this study indicate that a performance-based foundation design method, based on limiting horizontal displacements rather than soil strength, may be more appropriate for ZRB triggers for the load combinations considered.

Horizontal displacements of a skirted foundation under horizontal cyclic loading could be estimated as a function of shear strain based on element tests or numerical analysis or analytical solutions, similar to solutions developed to derive undrained settlement of circular foundations under vertical load (Osman & Bolton 2005). Further research is required to develop robust but simple solutions to derive horizontal displacement of skirted foundations from shear strain measurements.

Acknowledgements

This work forms part of the activities of the Centre for Offshore Foundation Systems (COFS), established in 1997 under the Australian Research Council's Special Research Centres Program and supported through the Fugro Chair in Geotechnics, the Lloyd's Register Foundation Chair and Centre of Excellence in Offshore Foundations and the Shell Chair in Offshore Engineering. The first and second authors were supported through ARC grant CE110001009. This support is gratefully acknowledged.

Accepted for publication in Ocean Engineering 21/05/2019
https://doi.org/10.1016/j.oceaneng.2019.05.044

7 References

Andersen K.H. (2015), Cyclic soil parameters for offshore foundation design, *Frontiers in Offshore Geotechnics III (ISFOG 2015)*, Oslo, Norway, 10-12 June 2015, Taylor and Francis, 5-82.

Britto A.M. & Kusakabe, O. (1982). Stability of unsupported axisymmetric excavations in soft clay. *Géotechnique*, 32 (3), 261-270.

Bruton, D. A.S., White, D.J., Carr, M., Cheuk, C.Y. (2008), Pipe-soil interaction during lateral buckling and pipeline walking: the Safebuck JIP, *In Proceedings Offshore Technology Conference*, Houston, USA, pp. OTC19589.

Bruton, D.A.S.., White, D.J., Cheuk, C.Y., Bolton, M.D., &and Carr, M.C. (2006). Pipe–soil interaction behaviour during lateral buckling, including large amplitude cyclic displacement tests by the Safebuck JIP. *In Proceedings Offshore Technology Conference*, Houston, OTC17944.

Caquot A. & Kerisel J. (1948). Tables for the calculation of passive pressure, active pressure and bearing pressure of foundations. Paris: Gauthier-Villars.

Cocjin M.L, Gourvenec S.M, White D.J. & Randolph M.F. (2014). Tolerably mobile subsea foundations – observations of performance. *Géotechnique*, 64 (11) 895–909.

Colreavy C., O' Loughlin, C.D. & Randolph, M.F. (2016). Experience with a dual pore pressure element piezoball. *International Journal of Physical Modelling in Geotechnics*, 16 (3), 101-118.

Dean, E.T.R., James, R.G., Schofield, A.N. and Tsukamoto, Y. (1998). Drum centrifuge study of three-leg jackup models on clay. *Géotechnique*, 48, 6, 761-785.

Dingle, H.R.C., White, D.J. and Gaudin, C. (2008). Mechanisms of pipe embedment and lateral breakout in soft clay. *Canadian Geotechnical Journal*, 45 (5), 636-652.

Dunnavant, T. W. and Kwan, C.-T. T. (1993). Centrifuge modelling and parametric analyses of drag anchor behavior. In Proceedings of the Offshore Technology Conference, Paper No. OTC-7202-MS.

Finnie, I.M.S. & Randolph, M.F. (1994). Punch-through and liquefaction induced failure of shallow foundations on calcareous sediments. *In Proceedings of the International Conference on Behavior of Offshore Structures*, BOSS '94, Boston, 4–7 July 1994, 217–230.

Garnier J., Gaudin C., Springman S.M., Culligan P.J., Goodings D., Konig D., Kutter B., Phillips R., Randolph M.F. & Thorel L. (2007). Catalogue of scaling laws and similitude questions in geotechnical centrifuge modelling. *International Journal of Physical Modelling in Geotechnics*, 7 (3), 1-23.

Gaudin C., O'Loughlin C.D., Hossain M.S., Randolph M.F. & Colliat J.L. (2014). Installation of suction caissons in Gulf of Guinea clay. *In Proceedings of 8th Int. Conf. on Physical Modelling in Geotechnics*,1, 493-499.

Gourvenec, S.M. & Mana, D.S.K. (2011). Undrained vertical bearing capacity factors for shallow foundations. *Géotechnique Letters*, 1: 101–108.

Gourvenec, S.M., Vulpe, C. & Murthy, T.G. (2014), A method for predicting the consolidated undrained bearing capacity of shallow foundation, *Géotechnique*, 64, 3, 215-225.

Jardine R.J & Standing J.R. (2012), Field axial cyclic loading experiments on piles driven in sand, *Soils and Foundations*, 52 (4), 723-736.

Jardine R.J., Andersen, K. & Puech, A. (2012). Cyclic loading of offshore piles: potential effects and practical design. *In Proceedings of the 7th International Conference on Offshore Site Investigations and Geotechnics*, Society for Underwater Technology, London, 59-100.

Krabbenhoft K., Lyamin A.V., Sloan S.W. (2007). Bounds to shakedown loads for a class of deviatoric plasticity models. *Computational Mechanics*, 39 (6), 879–888.

Larew, H.G. & Leonards, G.G. (1962). A strength criterion for repeated loads. *In Proceedings of the 41st Annual Meeting of the Highway Research Board*, Washington, D.C, 41, 526-556.

Levy N. H., Einav I. & Hull T. (2009). Cyclic shakedown of piles subjected to two-dimensional lateral loading. *International Journal for Numerical and Analytical Methods in Geomechanics*, 33, 1339-1361.

Mana D.S.K., Gourvenec S. M., Randolph M.F & Hossain M.S. (2012). Failure mechanisms of skirted foundations in uplift and compression, *International Journal of Physical Modelling in Geotechnics*, 12 (2), 47-62

Mana D.S.K., Gourvenec S.M. & Randolph M.F. (2013a). Experimental investigation of reverse end bearing of offshore shallow foundations. *Canadian Geotechnical Journal*, 2013, 50 (10), 1022-1033

Mana, D.S.K., Gourvenec, S. & Randolph, M.F., (2013b). A novel technique to mitigate the effect of gapping on the uplift capacity of offshore shallow foundations. *Géotechnique*, 63 (14), 1245-1252.

O'Beirne C., O'Loughlin C.D. & C. Gaudin (2017). Assessing the penetration resistance acting on a dynamically installed anchor in normally consolidated and overconsolidated clay. *Canadian Geotechnical Journal*, 2017, 54 (1): 1-17

Osman, A. S. & Bolton, M. D. (2005). Simple plasticity-based prediction of the undrained settlement of shallow circular foundations on clay. *Géotechnique*, 55 (6), 435–447.

Osman, A.S. & Randolph, M. F. (2012). An Analytical Solution for the Consolidation around a Laterally Loaded Pile. *International Journal of Geomechanics* 12 (3), 199– 208.

Peek, R. & Kristiansen N. (2009) Zero-radius bend method to trigger lateral buckles. *Journal of Transportation Engineering*, 135 (12), 946–952.

Randolph, M. F., Jewell, R. J., Stone, K. J. & Brown, T. A. (1991). Establishing a new centrifuge facility. *In Proceedings of the international conference on centrifuge modelling*, Centrifuge '91, Boulder (eds H.-Y. Ko and F. G. McLean), Rotterdam, the Netherlands: Balkema, 3–9.

Rimoy S., Jardine R.J. & Standing J.R. (2013). Displacement response to axial cycling of piles driven in sand. *Geotechnical Engineering*, 166 (GE2), 131-146

Sahdi F., Gaudin C., White D.J. & Boylan N (2014). Interpreting T-bar tests in ultra-soft clay, *International Journal of Physical Modelling in Geotechnics*, 14 (1), 13-19.

Skempton, A.W. (1951). The bearing capacity of clays. Building Research Congress, London, England, 180–189.

Stewart, D. P. & Randolph, M. F. (1991). A new site investigation tool for the centrifuge. *In Proceedings of international conference on centrifuge modelling*, Centrifuge '91, Boulder (eds H.-Y.Ko and F. G. McLean), Rotterdam, the Netherlands:Balkema, 531–538.

Stewart, D. P. (1992). Lateral loading of piled bridge abutments due to embankment construction. *PhD thesis*, The University of Western Australia, Perth, Australia.

Tani, K. & Craig, W.H. (1995). Bearing capacity of circular foundations on soft clay of strength increasing with depth. *Soils and Foundations*, 35 (4): 21–35.

Tika, Th.E. & Hutchinson, J.N. (1999). Ring shear tests on soil from the Vaiont landslide slip surface. *Géotechnique*, 49 (1), 59-74.

Tsuha C.H.C., Foray P.Y.., Jardine R.J., Yang Z.X., Silva M. & Rimoy SP. (2012). Behaviour of displacement piles in sand under cyclic axial loading. *Soils and Foundations*, 52: 393–410.

Vucetic, M. (1994). Cyclic Threshold Shear Strains in Soils. *Journal of Geotechnical Engineering*, ASCE 120 (12), 2208-2228.

Vulpe, C., Gourvenec, S.M. & Cornelius, A.F., (2017). Effect of embedment on consolidated undrained capacity of skirted circular foundations in soft clay under planar loading. *Canadian Geotechnical Journal*, 54 (2),158-172.

Watson, P.G. (1999). Performance of skirted foundation for offshore structures. *PhD thesis*, The University of Western Australia, Perth, Australia.

Yuan F., White D.J., & O'Loughlin C. (2017). The evolution of seabed stiffness during cyclic movement in a riser touchdown zone on soft clay, *Géotechnique*, 67 (2), 127-137.

Zakeri, A. Liedtke, E. Clukey, E.C. and Jeanjean, P. (2014). Long-term axial capacity of deepwater jetted piles, *Géotechnique*, 64 (12), 966-980.

Zografou, D., Gourvenec, S.M., & O'Loughlin C.D. (2019). Response of normally consolidated clay under irregular cyclic loading, *Géotechnique*, 69 (2), 106-121.

Accepted for publication in Ocean Engineering 21/05/2019
https://doi.org/10.1016/j.oceaneng.2019.05.044

Figure 1 A Zero-Radius Bend (ZRB) trigger prior to installation (from Peek & Kristiansen 2009)

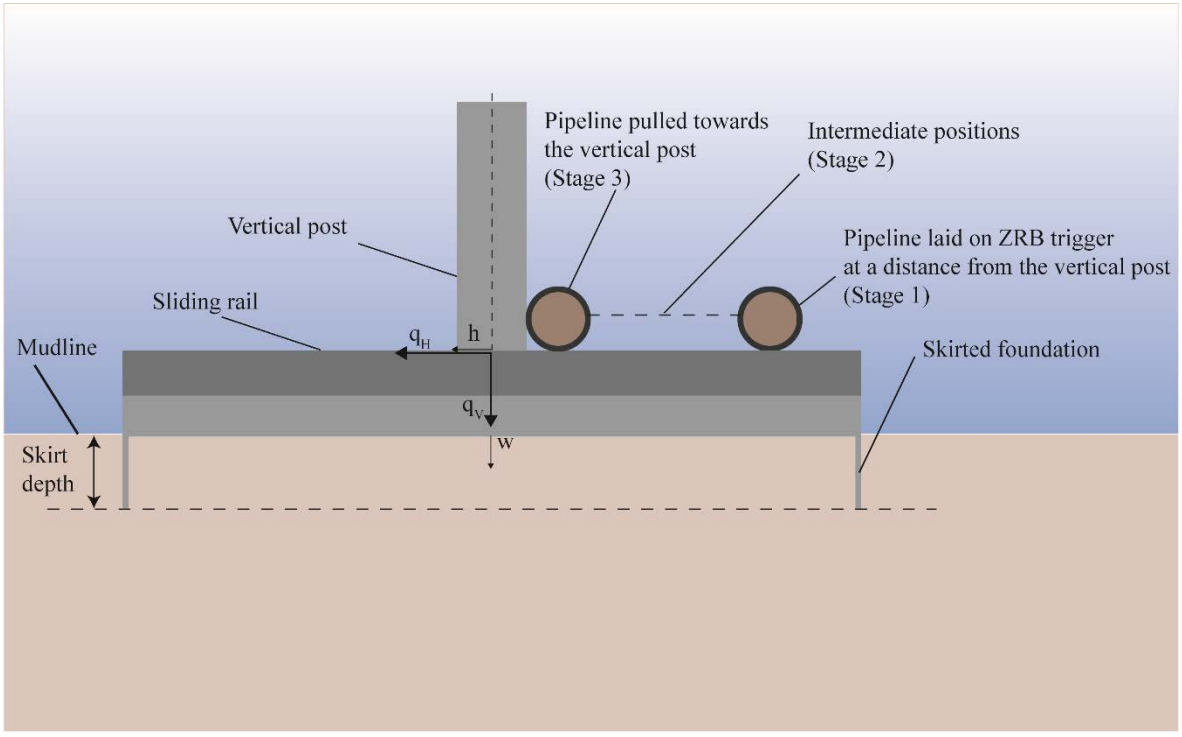

Figure 2 Schematic representation of a ZRB trigger with potential positions of the pipeline on the trigger during the pipe-laying procedure and sign convention for loads and displacements used in the model tests

Accepted for publication in Ocean Engineering 21/05/2019
https://doi.org/10.1016/j.oceaneng.2019.05.044

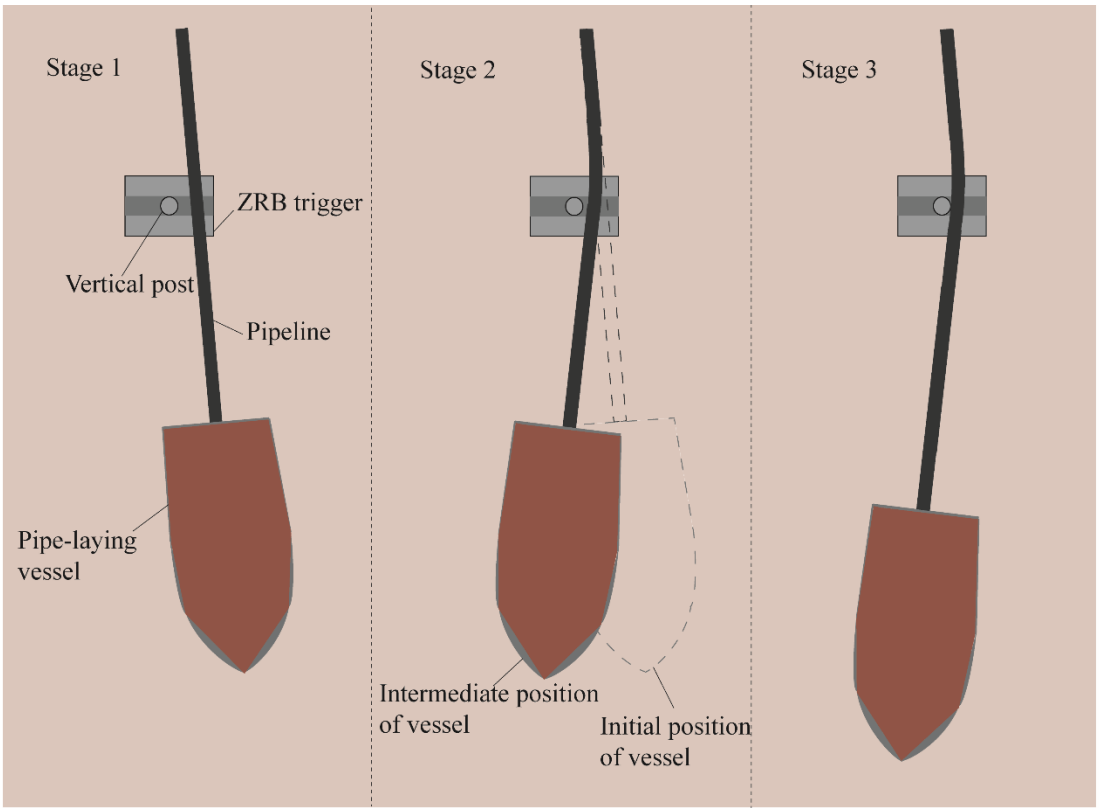

Figure 3 Schematic representation of pipe-laying procedure leading to loading on ZRB trigger: (a) Stage 1, pipeline is laid on the ZRB trigger, (b) Stage 2, pipe-laying vessel moves laterally towards the vertical post to create a small curvature on the pipeline and (c) Stage 3, the vessel moves forward and pipe-laying continues

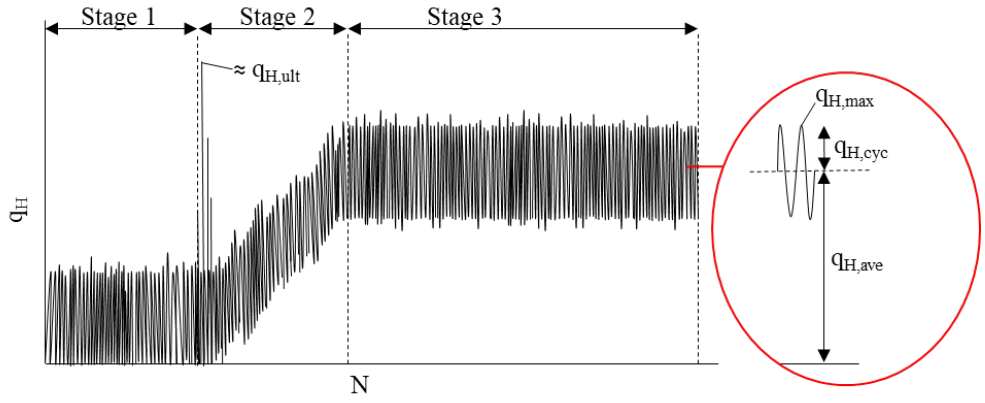

Figure 4 Representation of typical loading imposed on a ZRB trigger foundation during pipe laying

Accepted for publication in Ocean Engineering 21/05/2019
https://doi.org/10.1016/j.oceaneng.2019.05.044

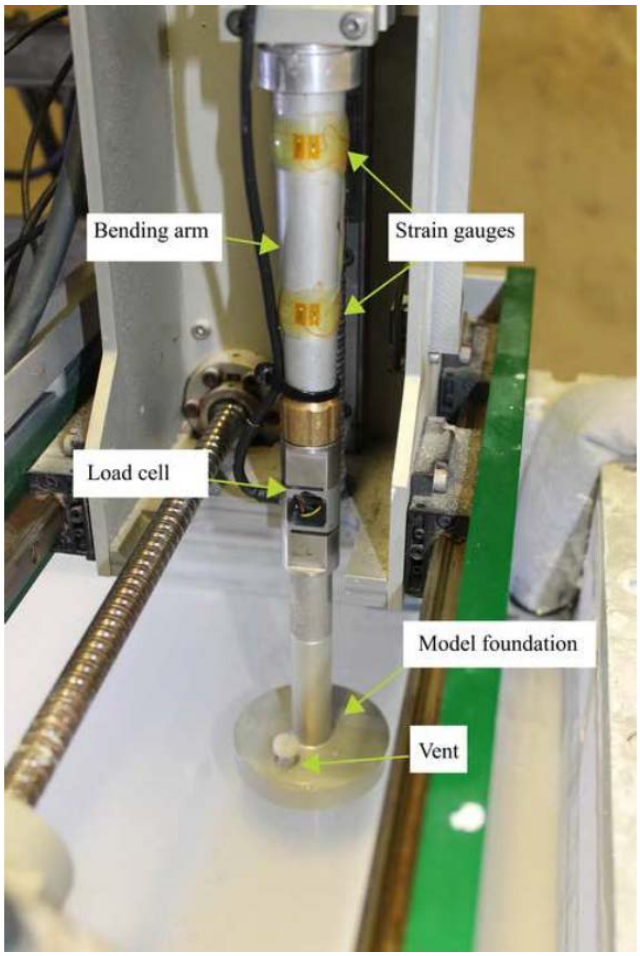

Figure 5 Experimental arrangement – model foundation connected to the actuator mounted over a sample of normally consolidated kaolin clay

Accepted for publication in Ocean Engineering 21/05/2019
https://doi.org/10.1016/j.oceaneng.2019.05.044

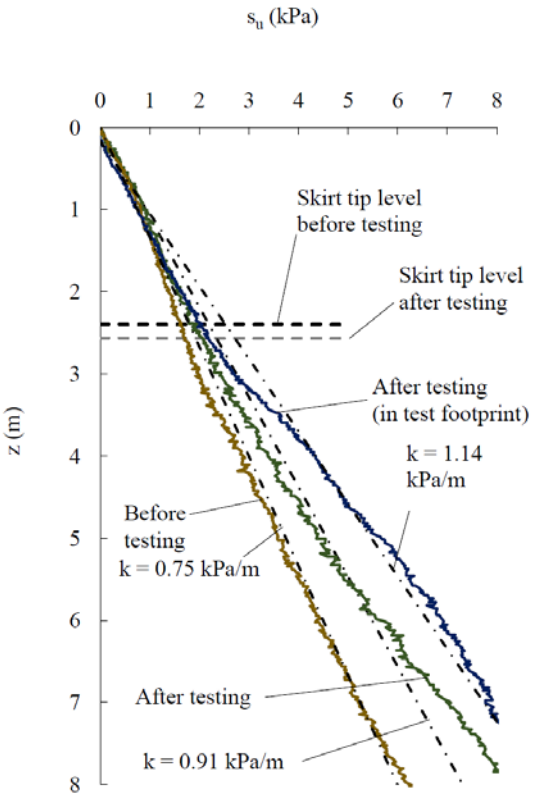

Figure 6 Profiles of undrained shear strength as assessed from T-bar tests

Accepted for publication in Ocean Engineering 21/05/2019
https://doi.org/10.1016/j.oceaneng.2019.05.044

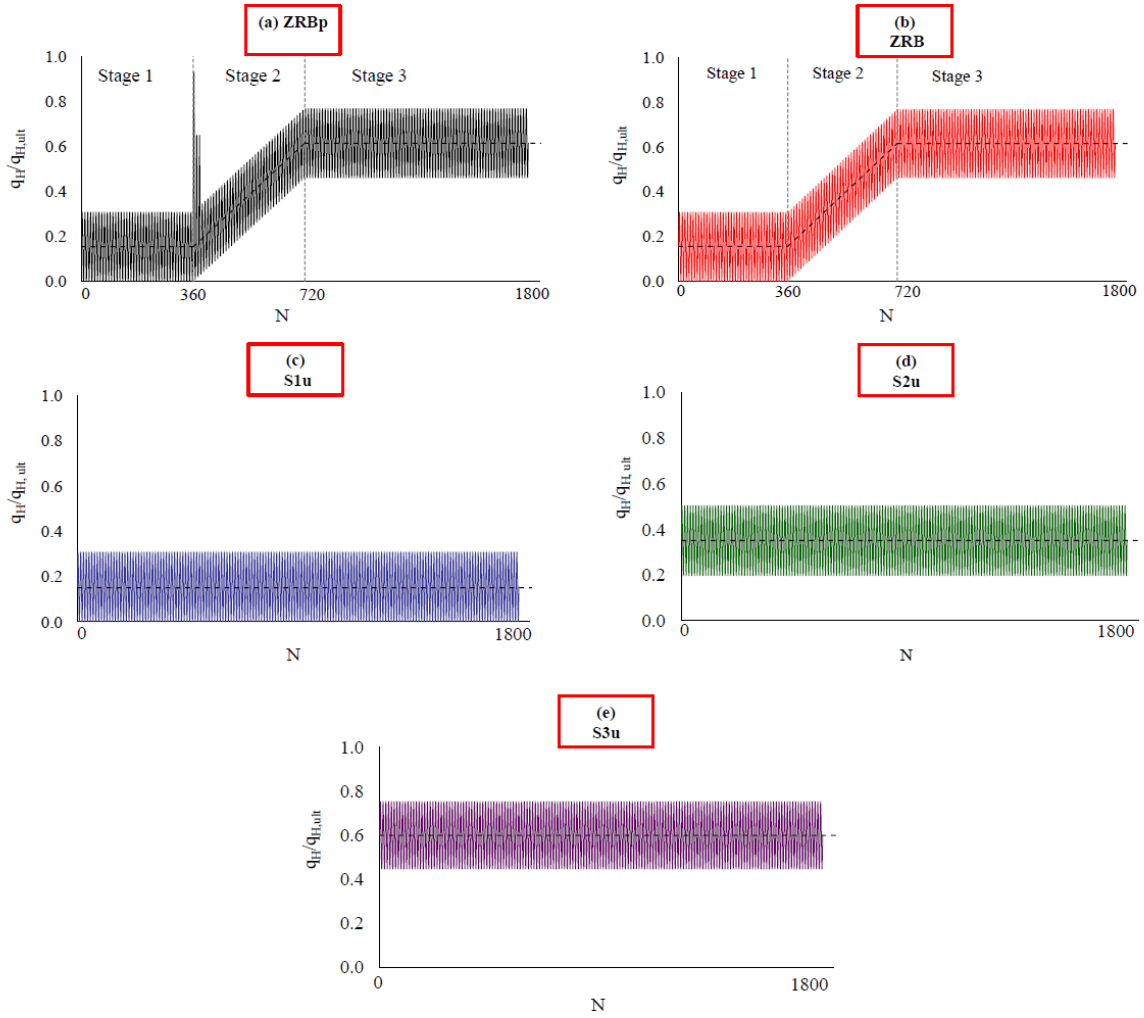

Figure 7 Schematic representation of the applied horizontal cyclic load sequences applied in centrifuge tests (a) ZRB sequence with peaks [ZRBp], (b) ZRB sequence [ZRB], (c) uniform load sequence of magnitude equivalent to Stage 1 in ZRB sequence [S1u] (d) uniform load sequence of magnitude equivalent to average magnitude of loading in Stage 2 in ZRB sequence [S2u] (e) uniform load sequence of magnitude equivalent to Stage 3 in ZRB sequence [S3u]

Accepted for publication in Ocean Engineering 21/05/2019
https://doi.org/10.1016/j.oceaneng.2019.05.044

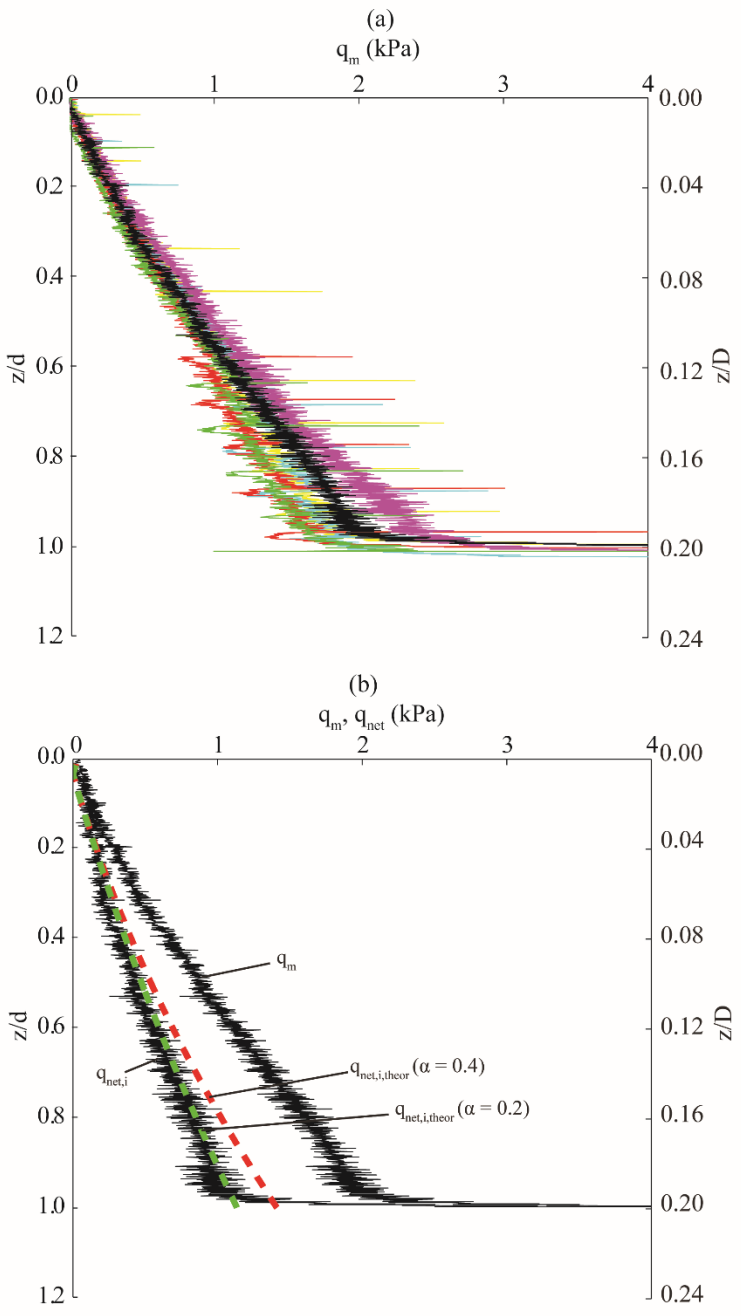

Figure 8 Installation resistance (a) measured in all tests and (b) compared with net and theoretical resistance (for example case, ZRBp)

Accepted for publication in Ocean Engineering 21/05/2019
https://doi.org/10.1016/j.oceaneng.2019.05.044

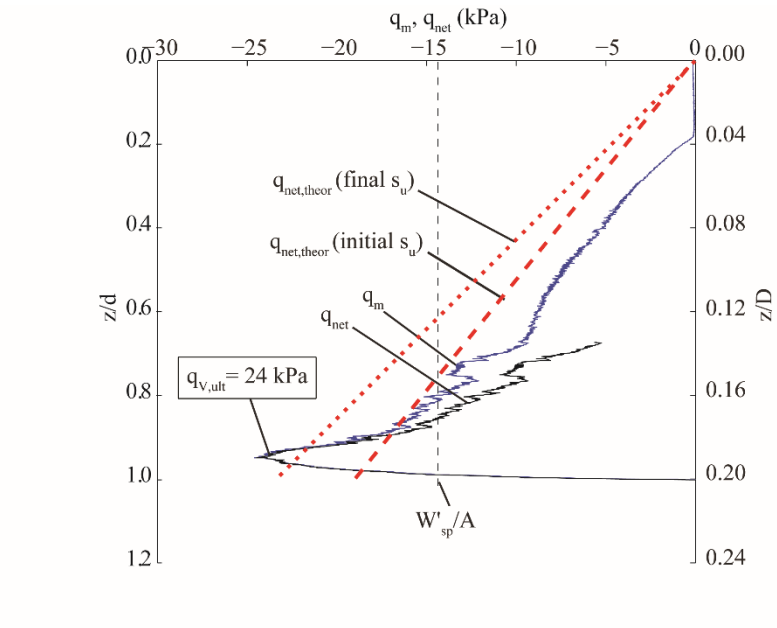

Figure 9 Measured vertical stress-embedment depth response and predicted vertical capacity based on initial and final (consolidated) undrained shear strength

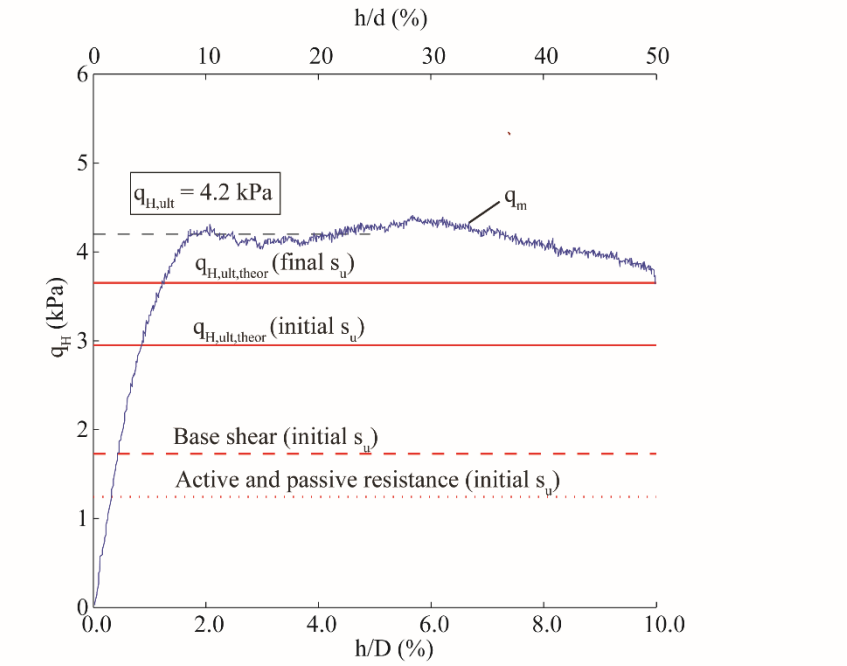

Figure 10 Measured horizontal stress-displacement response and predicted horizontal load capacity based on in situ and consolidated shear strength

Accepted for publication in Ocean Engineering 21/05/2019
https://doi.org/10.1016/j.oceaneng.2019.05.044

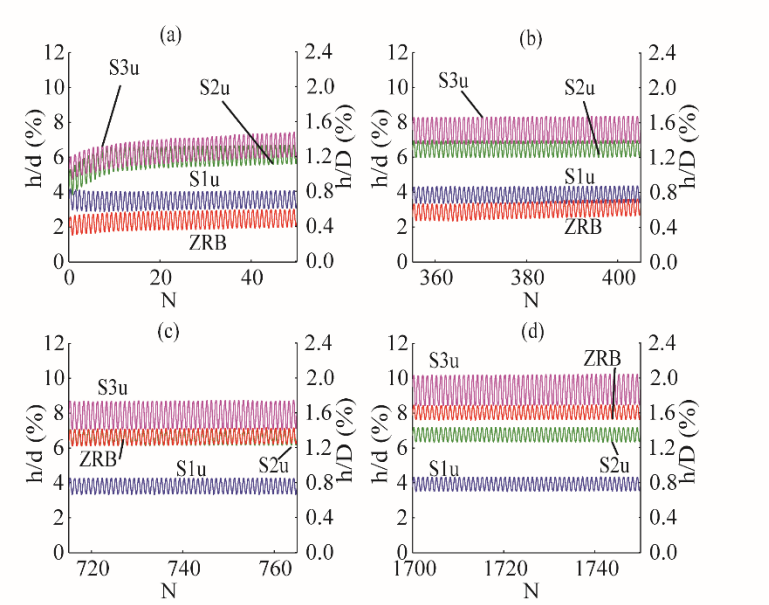

Figure 11 Normalised horizontal displacements in tests with ZRB loading sequence [ZRB], uniform Stage 1 loading [S1u], uniform Stage 2 loading [S2u], and uniform Stage 3 loading [S3u] at (a) beginning of Stage 1; N=0-50, (b) transition from Stage 1 to Stage 2; N=355-405, (c) transition from Stage 2 to Stage 3; N=715-765 and (d) end of Stage 3; N=1700-1750

Accepted for publication in Ocean Engineering 21/05/2019
https://doi.org/10.1016/j.oceaneng.2019.05.044

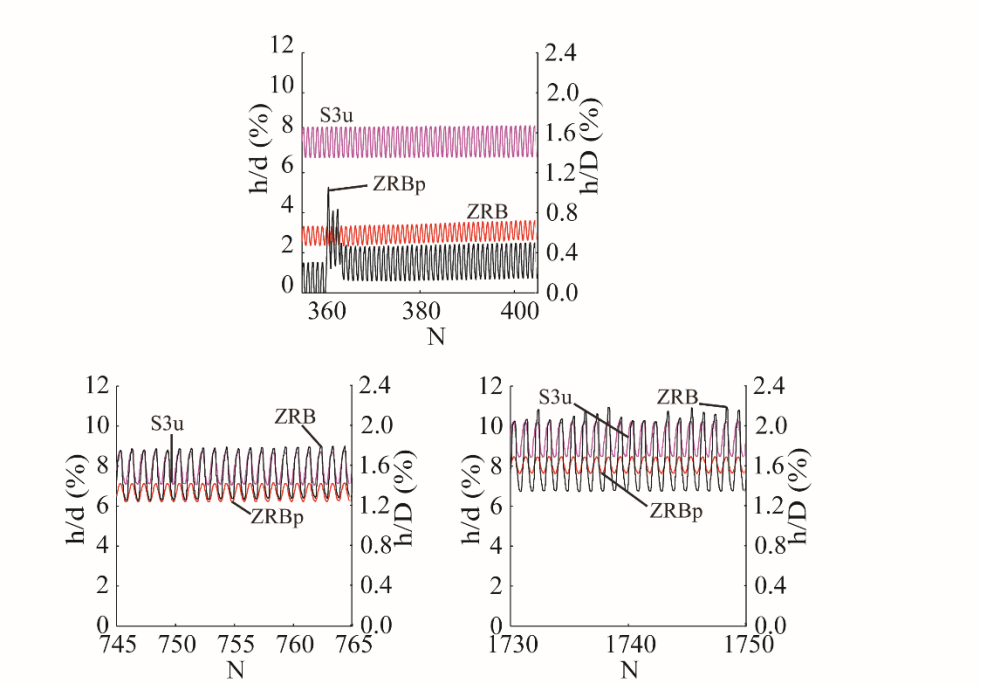

Figure 12 Normalised horizontal displacements in tests with uniform Stage 3 loading [S3u], ZRB loading sequence [ZRB] and ZRB loading sequence with peaks [ZRBp] at (a) transition from Stage 1 to Stage 2; N=355-405, (b) transition from Stage 2 to Stage 3; N=745-765 and (c) end of Stage 3; N=1730-1750

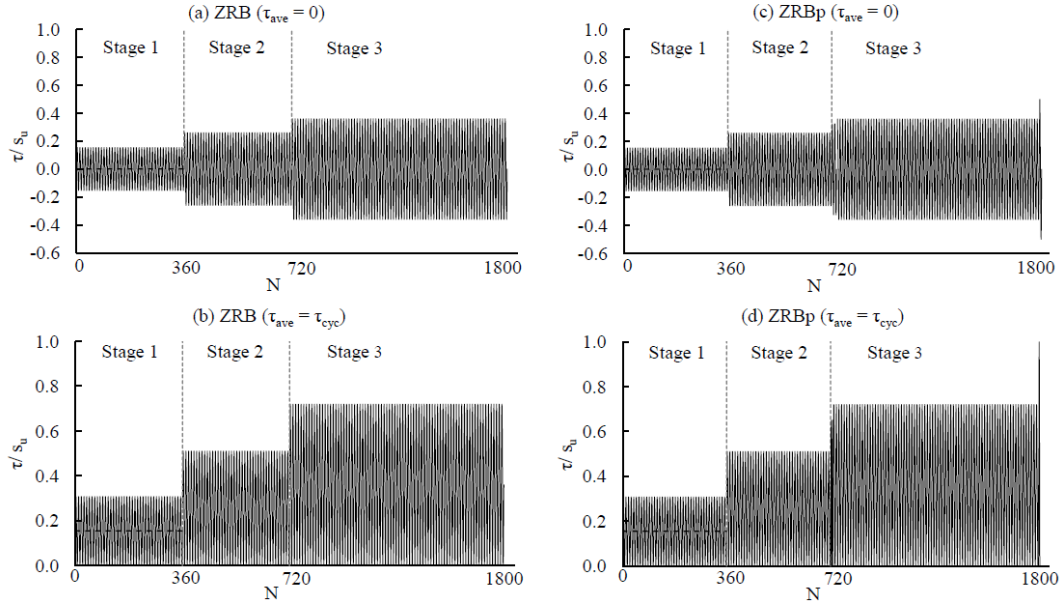

Figure 13 Schematic representation of alternatives for idealisation of ZRB loading sequence test as parcels of uniform amplitude for the purpose of the strain accumulation procedure in test ZRB as (a) two-way symmetrical cyclic loading, i.e. $\tau_{ave} = 0$ and (b) one-way non-symmetrical cyclic loading with $\tau_{ave} = \tau_{cyc}$, and in test ZRBp as (c) two-way symmetrical cyclic loading, i.e. $\tau_{ave} = 0$ and (d) one-way non-symmetrical cyclic loading with $\tau_{ave} = \tau_{cyc}$

Accepted for publication in Ocean Engineering 21/05/2019
https://doi.org/10.1016/j.oceaneng.2019.05.044

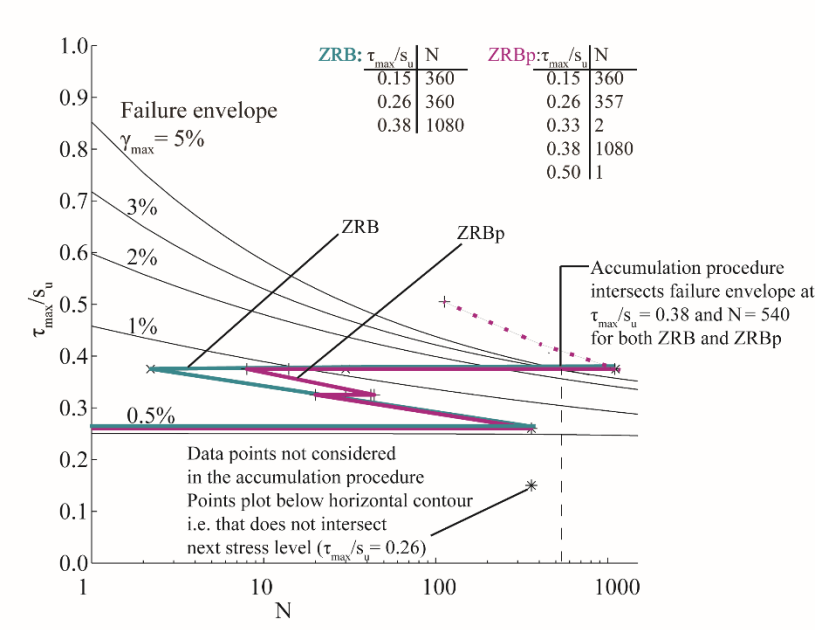

Figure 14 Accumulation procedure for symmetrical cyclic stress sequence idealisation representing ZRB loading sequence test [ZRB] and ZRB loading sequence with peaks test [ZRBp] on strain contour diagram from symmetrical cyclic DSS tests

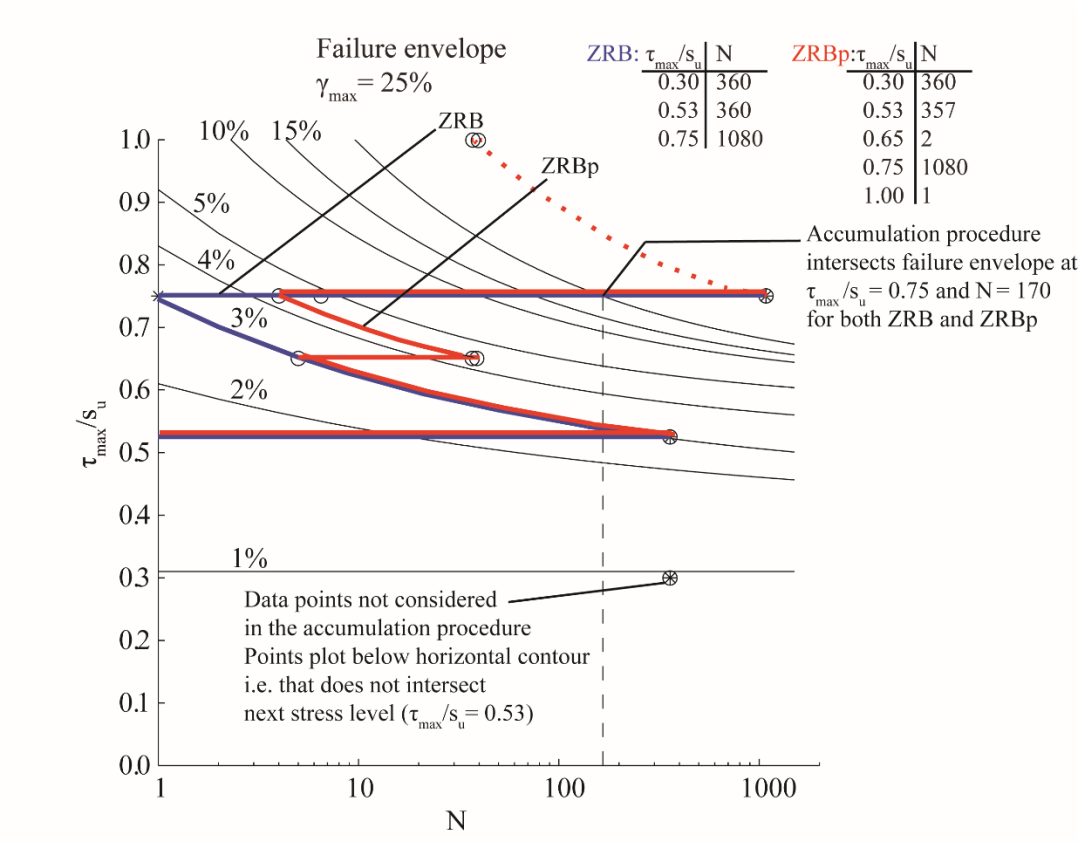

Figure 15 Accumulation procedure for non-symmetrical cyclic stress sequence idealisation representing ZRB loading sequence test [ZRB] and ZRB loading sequence with peaks test [ZRBp] on strain contour diagram from non-symmetrical cyclic DSS tests

Accepted for publication in Ocean Engineering 21/05/2019
https://doi.org/10.1016/j.oceaneng.2019.05.044

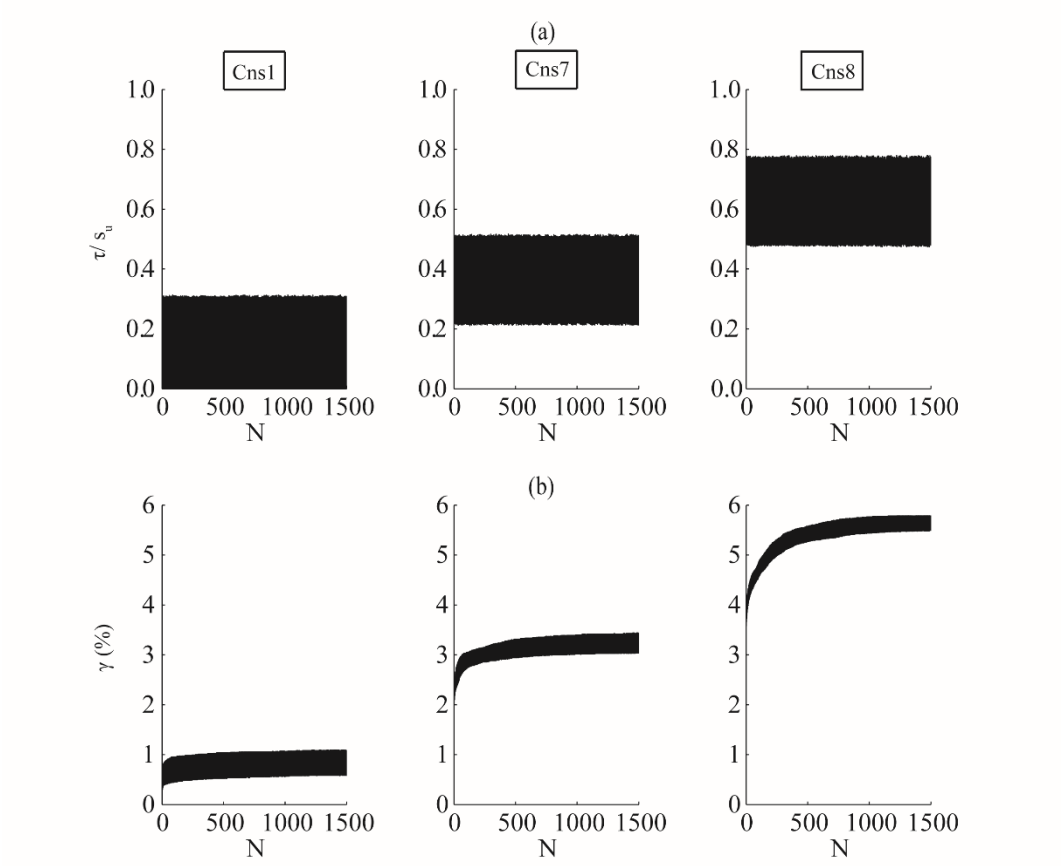

Figure 16 Cyclic DSS test results in normally consolidated kaolin (a) applied shear stress and (b) measured shear strains under $\tau_{ave}/s_u = 0.15$ and $\tau_{cyc}/s_u = 0.16$ (equivalent to S1u & Stage 1 in ZRB tests), $\tau_{ave}/s_u = 0.36$ and $\tau_{cyc}/s_u = 0.15$ (equivalent to S2u & Stage 2 in ZRB tests) and $\tau_{ave}/s_u = 0.62$ and $\tau_{cyc}/s_u = 0.16$ (equivalent to S3u & Stage 3 in ZRB tests)